IAES International Journal of Robotics and Automation (IJRA)
Vol. 15, No. 4, December 2026, pp. 745∼762
ISSN: 2722-2586, DOI: 10.11591/ijra.v15i4.pp745-762

Memory-aware adaptive multi-mode steering supervision for autonomous agricultural mobile robots

Athirah Najihah Zulkifili[1], Ismayuzri Ishak[1], Muhammad Aizzat Zakaria[1], Chuan Yu[2], Beng Jin[2]
[1]Faculty of Manufacturing and Mechatronic Engineering Technology, Universiti Malaysia Pahang Al-Sultan Abdullah, Pahang, Malaysia
[2]Pixel Intelligence Co., Ltd., Minato-ku, Tokyo, Japan

Article Info

Article history:

Received Jun 22, 2026
Revised Aug 14, 2026
Accepted Nov 10, 2026

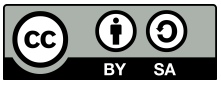
Keywords:

Adaptive steering supervision
Autonomous agricultural robots
Memory-aware control
Multi-mode steering
Path tracking

ABSTRACT

Frequent steering-mode transitions can reduce tracking consistency in multi-mode agricultural mobile robots. This study proposes a memory-aware adaptive supervisor that coordinates front-wheel steering, rear-wheel steering, counter-phase four-wheel steering, and Crab steering using curvature- and terrain-assisted arbitration, hysteresis, dwell-time protection, and separate turn-memory and recovery-memory states. Under the nominal benchmark, the proposed method reduced root mean square (RMS) cross-track error by 26.8%, accepted steering-mode transitions by 43.7%, and transition-window RMS wheel-steering rate by 22.3% compared with an equivalent non-memory supervisor. Disturbance tests under initial lateral offsets of 0.2 to 0.8 m produced tracking improvements of 24.2% to 26.1%. Across 20 paired Monte Carlo trials with random initial-position and heading perturbations, RMS cross-track error, accepted transitions, and transition-window RMS steering rate were reduced by 25.5%, 41.2%, and 22.0%, respectively, with all paired comparisons significant at $p < 0.001$. The results show that event-specific temporal memory improves tracking consistency, steering continuity, and disturbance recovery without online optimisation or policy learning. However, these results were obtained in a simulated environment using a kinematic vehicle model, and future work will validate the proposed supervisor on a physical robotic platform under field conditions.

This is an open access article under the CC BY-SA license.



Corresponding Author:

Ismayuzri Ishak
Faculty of Manufacturing and Mechatronic Engineering Technology, Universiti Malaysia Pahang Al-Sultan Abdullah
Pekan, Pahang, Malaysia
Email: ismayuzri@umpsa.edu.my

1. INTRODUCTION

The growth of precision agriculture has accelerated the deployment of autonomous agricultural vehicles and unmanned agricultural ground vehicles for spraying, harvesting, crop monitoring, and orchard navigation [1], [2]. Accurate path tracking is required to improve operational efficiency, reduce labour dependency, and minimise crop damage [2], [3]. However, uneven terrain, deformable surfaces, wheel slip, mud, narrow crop rows, and changing operating conditions can degrade steering stability and tracking accuracy [2], [4]. Accordingly, pure pursuit (PP), model predictive control (MPC), sliding mode control (SMC), and adaptive control methods have been investigated for agricultural navigation [1], [5]. Since these robots commonly op-

erate at low speed, kinematic models remain practical because of their computational efficiency and adequate accuracy under limited dynamic effects [2].

Multi-mode steering systems incorporating front-wheel steering (FWS), rear-wheel steering (RWS), four-wheel steering (4WS), and Crab steering can improve manoeuvrability in constrained agricultural environments [6], [7]. These configurations provide complementary characteristics under different path and manoeuvring conditions [8], while adaptive mode selection can improve spatial utilisation and steering flexibility [7], [9]. However, no fixed configuration is consistently optimal over a route containing straight, curved, and lateral-correction regions. A supervisory strategy is therefore required to coordinate mode selection while preserving continuity during transitions.

Existing geometric, model-based, fuzzy, predictive, and learning-based methods improve path tracking, disturbance rejection, steering coordination, or mode selection [10], [11]. Learning-based navigation has also been applied to agricultural robots using multiple steering configurations [12]. Nevertheless, these approaches commonly rely on instantaneous vehicle states, predicted responses, or learned actions, with limited explicit retention of recent turning and recovery context.

Abrupt or repetitive transitions between steering configurations may cause discontinuous steering allocation, oscillatory behaviour, and tracking degradation [13], [14]. Hysteresis separates mode-entry and mode-exit thresholds [15], but fixed thresholds cannot account for persistent disturbances. In rutted crop furrows, uneven terrain and wheel slip may repeatedly drive curvature and tracking errors across both thresholds, causing oscillatory mode shifts and reduced clearance from crops or furrow boundaries [2], [4].

Dwell time limits rapid transitions but cannot distinguish temporary fluctuations from genuine manoeuvring changes. A short dwell time may not suppress terrain-induced switching, whereas a long dwell time may delay CP4WS activation at a tight headland turn or retain it after the turn. Thus, neither mechanism preserves recent turning or recovery context, allowing premature mode release and reactivation. Although hierarchical and smooth-switching methods improve transition coordination [16], [17], event-specific retention of turning and recovery context remains insufficiently addressed. Table 1 summarises the representative approaches.

Table 1. Comparison of representative steering supervisory approaches

Method	Adaptive	Multi-mode	Continuity	Stability	Recovery
PP-based control [10]	✗	✗	✗	✓	✗
Fuzzy MPC [18]	✓	✗	✗	✓	✗
Adaptive MPC [11]	✓	✓	✗	✓	✗
Learning-based mode switching [14]	✓	✓	✗	✓	✗
Hierarchical switching [16]	✓	✓	✓	✓	✗
Smooth switching [17]	✓	✓	✓	✓	✗
Switched-system control [19]	✗	✓	✓	✓	✗
Proposed memory-aware framework	✓	✓	✓	✓	✓

Note: ✓ indicates that the corresponding feature is explicitly incorporated or evaluated, whereas ✗ indicates that it is not explicitly addressed. Recovery refers to explicit post-disturbance recovery support or evaluation.

In this study, memory-aware supervision refers to finite-duration retention of recent turning and disturbance-recovery conditions for subsequent steering-mode decisions. Unlike hysteresis, which separates entry and exit thresholds, and dwell time, which limits the timing of successive transitions, the proposed memory states preserve recent manoeuvring context after the instantaneous triggering condition has decreased.

The scientific question addressed in this study is whether event-specific supervisory memory can improve trajectory-tracking consistency, reduce unnecessary steering-mode transitions, and strengthen disturbance recovery compared with adaptive multi-mode steering supervision without temporal memory.

A memory-aware adaptive supervisory framework is therefore proposed for low-speed autonomous agricultural mobile robots. The framework integrates FWS, RWS, counter-phase four-wheel steering (CP4WS), and Crab steering with curvature-based arbitration, terrain assistance, hysteresis, dwell-time protection, condition-dependent velocity scheduling, and separate turn-memory and recovery-memory states.

The novelty lies in integrating distinct finite-duration states for recent turning and disturbance recovery into multi-mode steering arbitration. These states retain whether steering support was recently required and use that context in subsequent supervisory decisions.

The main contributions are: i) A unified multi-mode steering architecture integrating FWS, RWS, CP4WS, and Crab steering for low-speed agricultural mobile robots. ii) An event-specific memory-aware supervisory mechanism that separately retains recent turning and disturbance-recovery conditions. and iii) A simulation-based evaluation against fixed steering modes and an equivalent non-memory supervisor using trajectory-tracking, wheel-level steering-transition, disturbance-recovery, parameter-sensitivity, and paired statistical-validation metrics.

a. Background and related work

– Kinematic modeling and multi-mode steering systems

Kinematic vehicle models are widely used for low-speed agricultural navigation because they provide adequate accuracy with low computational demand while neglecting detailed tyre-force and lateral-slip dynamics [20], [21]. They have been applied with PP, MPC, and related path-tracking methods in autonomous agricultural vehicles and mobile robots [21], [22]. These studies demonstrate that kinematic formulations provide a practical balance between tracking performance and computational efficiency [23].

Configurable and multi-mode steering systems improve manoeuvrability by supporting different front- and rear-wheel coordination patterns [24], [25]. Such systems can enhance navigation adaptability and trajectory tracking compared with conventional single-mode steering [24], [26]. FWS supports conventional forward motion, RWS improves low-speed manoeuvrability, CP4WS reduces the effective turning radius through counter-phase axle coordination [27], and Crab steering enables lateral or oblique motion with limited heading change [26]. Coordinated steering strategies can also improve wheel-command consistency and turning-radius regulation [24], [25], [28]. Because these modes provide complementary capabilities, a supervisor is required to select and transition between them without abrupt or repetitive switching.

– Supervisory steering arbitration and memory continuity

PP remains widely adopted for low-speed agricultural navigation because of its simple geometric formulation and low computational demand [29], [30]. Adaptive look-ahead selection, optimisation-based tuning, and curvature-aware extensions improve tracking within an active steering configuration [30], [31], but do not directly address coordination among multiple steering modes.

Supervisory steering methods coordinate mode selection and steering allocation according to path geometry, vehicle states, and manoeuvring demand [32], [33]. Switching-based, adaptive, and hierarchical approaches improve manoeuvrability and robustness in multi-mode and steer-by-wire systems [32]-[34]. However, many rely primarily on instantaneous measurements or predicted responses rather than retained manoeuvring context.

Hysteresis reduces repeated switching near decision boundaries by separating activation and release conditions [15], [35], while dwell time enforces a minimum interval between accepted transitions [36], [37]. Overlapping switching regions can further reduce sensitivity to small changes around mode boundaries [38], and memory-dependent switching demonstrates that recent conditions can be incorporated into later supervisory decisions [39].

Nevertheless, hysteresis and dwell time do not explicitly preserve whether turning or recovery support was recently required. Hysteresis modifies the switching boundaries, whereas dwell time restricts transition timing. A finite-duration memory state instead retains event-specific context after curvature or tracking error has fallen below its activation threshold, thereby reducing premature mode release and repeated reactivation.

Motivated by this distinction, the proposed supervisor combines hysteresis, dwell-time protection, and separate turn-memory and recovery-memory states. The framework is evaluated on a synthetic benchmark containing straight, moderate-curvature, high-curvature, and terrain-slope variations.

2. RESEARCH METHOD

The proposed framework combines a unified low-speed kinematic vehicle model, Pure Pursuit path tracking, multi-mode steering mapping, condition-dependent velocity scheduling, and memory-aware steering arbitration. The supervisor selects among front-wheel steering (FWS), rear-wheel steering (RWS), counter-phase four-wheel steering (CP4WS), and Crab steering according to path curvature, tracking errors, terrain slope, hysteresis, dwell-time constraints, and finite-duration turn-memory and recovery-memory states. Figure 1 summarises the overall architecture.

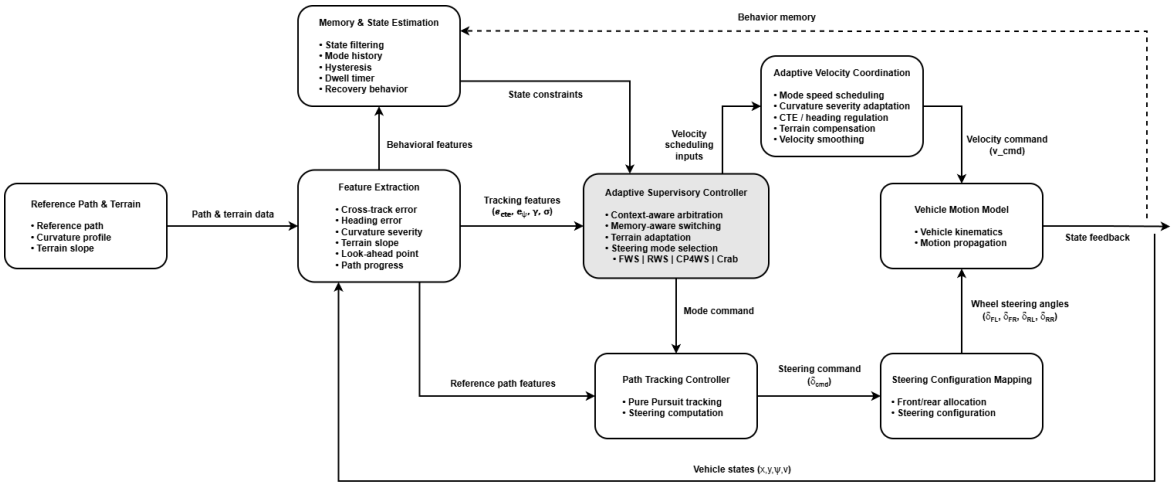


Figure 1. Overall architecture of the proposed memory-aware adaptive steering framework

2.1. Vehicle kinematic model

The Pixkit 2.0 platform shown in Figure 2 was used as the geometric reference for the wheelbase and track-width parameters adopted in the simulation. The platform was not physically tested in this study. The steering configurations considered in the unified model are shown in Figure 3. Figure 3(a) shows front-wheel steering (FWS), in which only the front wheels steer, while Figure 3(b) shows rear-wheel steering (RWS), in which only the rear wheels steer. Figure 3(c) shows counter-phase four-wheel steering (CP4WS), in which the front and rear wheels steer in opposite directions, and Figure 3(d) shows Crab steering, in which the front and rear wheels steer in the same direction for diagonal motion.



Figure 2. Pixkit 2.0 platform used as the geometric reference for simulation parameterisation

The low-speed vehicle motion was represented by

$$\begin{aligned} \dot{x} &= v\cos(\psi+\beta), \\ \dot{y} &= v\sin(\psi+\beta), \\ \dot{\psi} &= \frac{v}{L}\left[\tan(\delta_f)-\tan(\delta_r)\right], \end{aligned} \tag{1}$$

where x and y denote the vehicle position, v is the commanded velocity, ψ is the heading angle, L is the wheelbase, and δ_f and δ_r are the equivalent front- and rear-axle steering angles.

The equivalent axle angles and steering-induced kinematic orientation offset were calculated as

$$\begin{aligned} \delta_f &= \tan^{-1}\left[\frac{\tan(\delta_{FL})+\tan(\delta_{FR})}{2}\right], \\ \delta_r &= \tan^{-1}\left[\frac{\tan(\delta_{RL})+\tan(\delta_{RR})}{2}\right], \\ \beta &= \tan^{-1}\left[\frac{\tan(\delta_f)+\tan(\delta_r)}{2}\right]. \end{aligned} \tag{2}$$

The reference point was assumed to lie approximately midway between the two axles. Therefore, β represents a steering-induced kinematic offset rather than tyre side-slip associated with lateral tyre dynamics. This approximation enables the lateral-motion characteristics of CP4WS and Crab steering to be represented within a computationally efficient low-speed model. The vehicle and simulation parameters are summarised in Table 2.

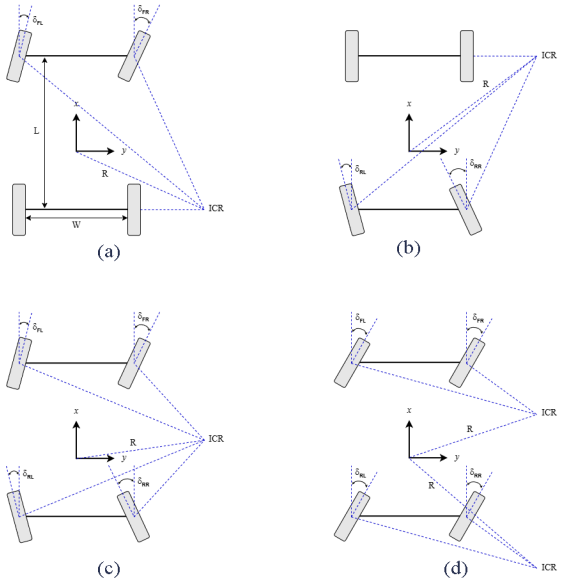


Figure 3. Steering configurations used in this study: (a) FWS, (b) RWS, (c) CP4WS, and (d) Crab steering

Table 2. Vehicle and simulation parameters

Parameter	Symbol	Value
Vehicle track width	W	1.47 m
Vehicle wheelbase	L	1.90 m
Rear steering gain	k_{rear}	1.0
Rear-wheel steering gain	k_{rws}	0.7
Nominal maximum speed	v_{max}	0.8 m/s
Sampling time	T_s	0.005 s

2.2. Pure pursuit and multi-mode steering mapping

The pure pursuit controller determines the target direction, wrapped heading error, curvature command, and steering command as

$$\begin{aligned} \theta &= \operatorname{atan2}\left(y_L - y_m,\, x_L - x_m\right), \\ \alpha &= \operatorname{wrapToPi}\left(\theta - \psi\right), \\ \kappa_{pp} &= \frac{2\sin(\alpha)}{L_d}, \\ \delta_{cmd} &= \tan^{-1}\left(L\kappa_{pp}\right), \end{aligned} \tag{3}$$

where (x_m, y_m) is the vehicle position, (x_L, y_L) is the look-ahead target, α is the wrapped heading error, and L_d is the look-ahead distance.

Mode-dependent look-ahead distances were assigned as

$$L_d = \begin{cases} 2.5\ \text{m}, & \text{FWS}, \\ 2.0\ \text{m}, & \text{RWS}, \\ 1.5\ \text{m}, & \text{CP4WS}, \\ 2.0\ \text{m}, & \text{Crab}. \end{cases} \tag{4}$$

These values and the global path re-acquisition mechanism were applied identically to the full supervisor without temporal memory (C7) and the memory-aware full supervisor (C8).

The equivalent front- and rear-axle steering commands were assigned as

$$\begin{aligned} \text{FWS}: &\quad (\delta_f, \delta_r) = (\delta_{cmd}, 0), \\ \text{RWS}: &\quad (\delta_f, \delta_r) = (0, -k_{rws}\delta_{cmd}), \\ \text{CP4WS}: &\quad (\delta_f, \delta_r) = (\delta_{cmd}, -k_{rear}\delta_{cmd}), \\ \text{Crab}: &\quad (\delta_f, \delta_r) = (\delta_{cmd}, k_{rear}\delta_{cmd}). \end{aligned} \tag{5}$$

Under the adopted sign convention, negative rear-axle steering represents counter-phase motion, whereas positive rear-axle steering represents same-phase motion.

For FWS, RWS, and CP4WS, Ackermann geometry was used to obtain the inner and outer wheel angles:

$$R = \frac{L}{\tan(|\delta|)}, \qquad \delta_{in,out} = \tan^{-1}\left[\frac{L}{R \mp W/2}\right]. \tag{6}$$

The inner and outer assignments depend on the turning direction. Crab steering instead uses parallel wheel commands:

$$\delta_{FL} = \delta_{FR} = \delta_f, \qquad \delta_{RL} = \delta_{RR} = \delta_r. \tag{7}$$

2.3. Condition-dependent velocity scheduling

The supporting velocity scheduler reduces tracking demand during increased curvature, tracking error, heading error, and terrain slope. Mode-dependent nominal speeds of 0.80, 0.65, 0.50, and 0.35 m/s were assigned to FWS, RWS, CP4WS, and Crab steering, respectively.

The condition-dependent terms were defined as

$$\begin{aligned} v_{severity} &= v_{max} - k_s\gamma, \\ v_{cte} &= v_{max} - k_c|e_{cte}|, \\ v_{\psi} &= v_{max} - k_{\psi}|e_{\psi}|, \\ v_{slope} &= v_{max} - k_{\sigma}\sigma, \end{aligned} \tag{8}$$

where γ is curvature severity, e_{cte} is cross-track error, e_{ψ} is heading error, and σ is terrain slope.

The final velocity command was obtained from

$$v_{cmd} = \text{sat}_{[v_{min}, v_{max}]}\left(w_1 v_{mode} + w_2 v_{severity} + w_3 v_{cte} + w_4 v_{\psi} + w_5 v_{slope}\right), \tag{9}$$

where $v_{min} = 0.25$ m/s and $v_{max} = 0.80$ m/s. Low-pass filtering and rate limiting were applied to prevent abrupt velocity changes.

Command smoothness was quantified using

$$J_{v,\text{RMS}} = \sqrt{\frac{1}{N-1}\sum_{k=2}^{N}\left[v_{cmd}(k) - v_{cmd}(k-1)\right]^2}, \tag{10}$$

where N is the number of commanded-velocity samples. All velocity-scheduling settings were identical for the Full Supervisor without Temporal Memory (C7) and the Memory-Aware Full Supervisor (C8), thereby ensuring that velocity scheduling did not confound the evaluation of temporal memory.

2.4. Adaptive and memory-aware steering arbitration

The supervisor uses curvature severity as the primary mode-selection variable, while tracking errors and terrain slope provide supplementary assistance. CP4WS is prioritised under severe curvature and large heading-recovery demand, RWS is used for moderate curvature and recovery support, and Crab steering is restricted to safe low-curvature lateral correction. Figure 4 summarises the arbitration process.

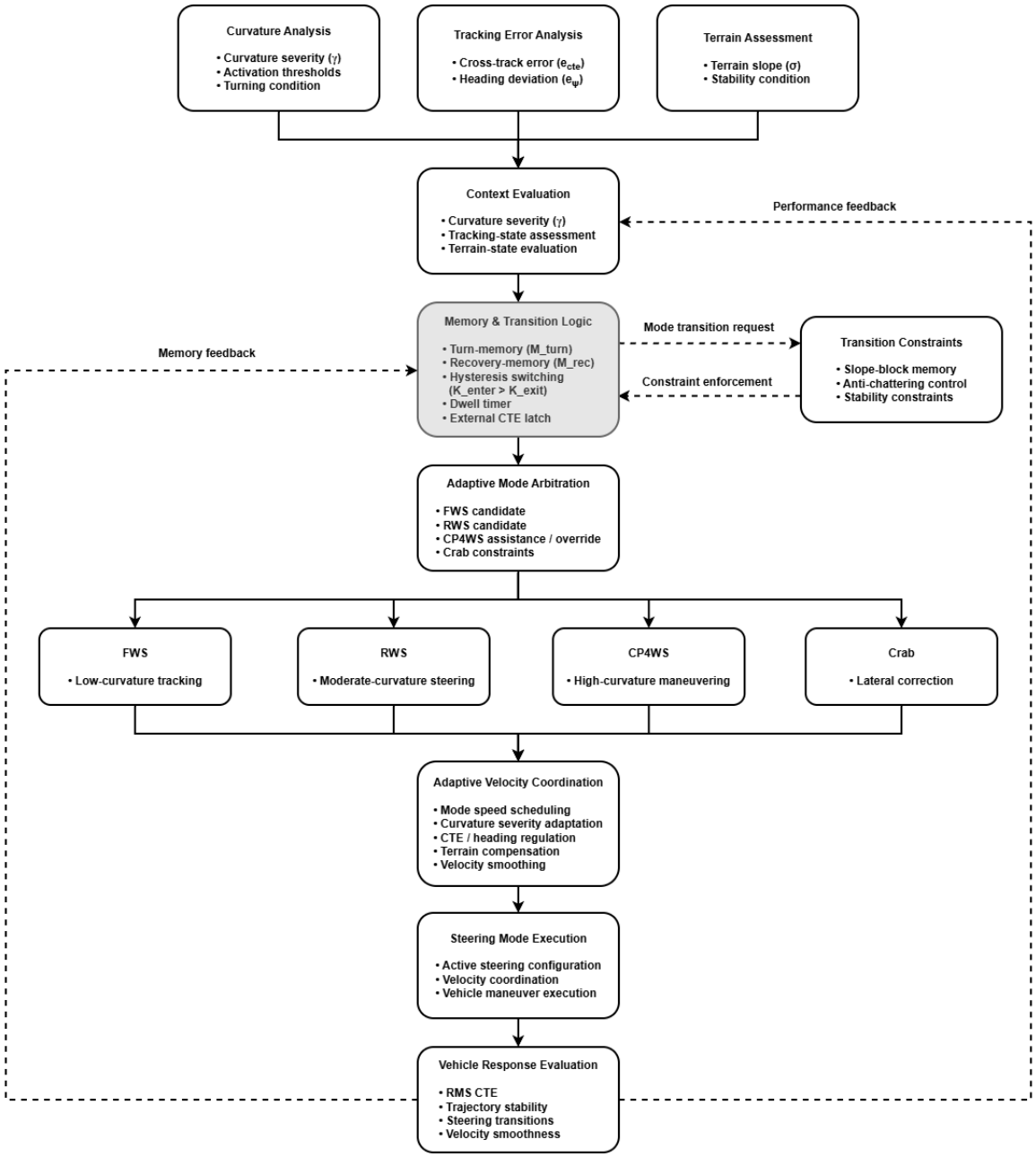


Figure 4. Supervisory decision-making process of the adaptive steering controller

The global curvature threshold was defined as

$$\kappa_{th} = 0.15\ \mathrm{m}^{-1}. \tag{11}$$

Separate activation and release thresholds satisfy

$$K_{enter} > K_{exit}, \tag{12}$$

while a minimum dwell time of $T_{dwell} = 0.60$ s prevents rapid consecutive accepted transitions. Hysteresis separates mode-entry and mode-exit conditions, whereas dwell time limits the timing of successive transitions. The proposed memory states additionally preserve recent event context after the instantaneous triggering condition decreases.

Turn memory is activated when curvature exceeds the RWS activation threshold or when the previous mode corresponds to RWS or CP4WS:

$$M_{turn}(k) = \begin{cases} N_{turn}, & \gamma(k) > K_{RWS,enter} \\ & \text{or } mode(k-1) \in \{\text{RWS}, \text{CP4WS}\}, \\ \max\left[M_{turn}(k-1) - 1,\, 0\right], & \text{otherwise.} \end{cases} \tag{13}$$

Recovery memory is activated by sufficiently large lateral or heading error:

$$M_{rec}(k) = \begin{cases} N_{rec}, & |e_{cte}| > e_{rec} \text{ or } |e_{\psi}| > \psi_{rec}, \\ \max\left[M_{rec}(k-1) - 1,\, 0\right], & \text{otherwise.} \end{cases} \tag{14}$$

The corresponding binary indicators are

$$I_{turn}(k) = \begin{cases} 1, & M_{turn}(k) > 0, \\ 0, & M_{turn}(k) = 0, \end{cases} \qquad I_{rec}(k) = \begin{cases} 1, & M_{rec}(k) > 0, \\ 0, & M_{rec}(k) = 0. \end{cases} \tag{15}$$

Turn memory retains recent turning support after curvature decreases, whereas recovery memory retains recent tracking-error context after the error returns below its activation threshold. Recovery support is restricted to moderate-curvature conditions and is suspended during active turn memory to avoid conflicting decisions.

Safety and eligibility rules disable Crab steering when terrain slope, curvature severity, heading error, or lateral error exceeds its safe range. Severe-curvature and heading-recovery conditions override lower-priority lateral-correction and memory actions. Table 3 summarises the resulting priority order.

Table 3. Priority order of the memory-aware steering-mode arbitration

Priority	Condition category	Selected action
1	Severe-curvature override	CP4WS
2	Large heading-recovery demand	CP4WS
3	Combined curvature and heading demand	CP4WS
4	Safe low-curvature lateral correction	Crab
5	Normal high-curvature condition	CP4WS
6	Normal moderate-curvature condition	RWS
7	Active turn memory	Retain turning support
8	Active recovery memory	Apply recovery support
9	Otherwise	FWS

The principal supervisory parameters are listed in Table 4. The curvature thresholds were selected through preliminary simulation tuning while preserving $K_{enter} > K_{exit}$. Turn-memory duration, recovery-memory duration, dwell time, and velocity-scheduling gain scale were subsequently evaluated through the one-factor-at-a-time sensitivity analysis reported in section 3.6. The selected turn-memory duration of 1800 samples, equivalent to 9.0 s, provided near-best tracking and transition suppression without unnecessarily prolonged turning support.

Table 4. Principal supervisory and memory parameters

Parameter	Symbol	Value
Global curvature threshold	κ_{th}	$0.15\ \text{m}^{-1}$
CP4WS entry threshold	$K_{CP,enter}$	$0.090\ \text{m}^{-1}$
CP4WS exit threshold	$K_{CP,exit}$	$0.0525\ \text{m}^{-1}$
RWS entry threshold	$K_{RWS,enter}$	$0.0525\ \text{m}^{-1}$
RWS exit threshold	$K_{RWS,exit}$	$0.030\ \text{m}^{-1}$
Minimum dwell time	T_{dwell}	0.60 s
Turn-memory duration	$N_{turn}T_s$	9.0 s
Recovery-memory duration	$N_{rec}T_s$	4.0 s

2.5. Simulation design and evaluation procedure

Eight benchmark cases were evaluated under a common synthetic trajectory, vehicle model, controller, and simulation configuration. C5 uses curvature-based supervision, C6 adds tracking-error assistance, C7 applies the complete terrain-assisted supervisor without temporal memory, and C8 adds the proposed turn-memory and recovery-memory states. The C7–C8 comparison therefore isolates the specific effect of memory-aware arbitration. The benchmark cases are summarised in Table 5.

Table 5. Simulation benchmark cases

Case	Strategy	Description
C1	Fixed FWS	Baseline front-wheel steering
C2	Fixed RWS	Baseline rear-wheel steering
C3	Fixed CP4WS	Baseline counter-phase steering
C4	Fixed Crab	Baseline lateral steering
C5	Supervisor Curvature	Curvature-based supervision
C6	Supervisor Curvature + CTE	Curvature and tracking-error supervision
C7	Full Supervisor (No Memory)	Adaptive supervision without temporal memory
C8	Full Supervisor (Memory-Aware)	Proposed memory-aware supervision

A synthetic benchmark trajectory was constructed with straight segments, moderate-curvature regions, high-curvature turns, and prescribed terrain-slope variations. The trajectory was designed to activate the steering and supervisory conditions under repeatable simulation settings and was not derived from field measurements or GIS data. Figure 5 presents the synthetic benchmark and its prescribed conditions. Figure 5(a) shows the three-dimensional trajectory, Figure 5(b) shows the path-curvature profile and supervisory thresholds, and Figure 5(c) shows the terrain-slope profile.

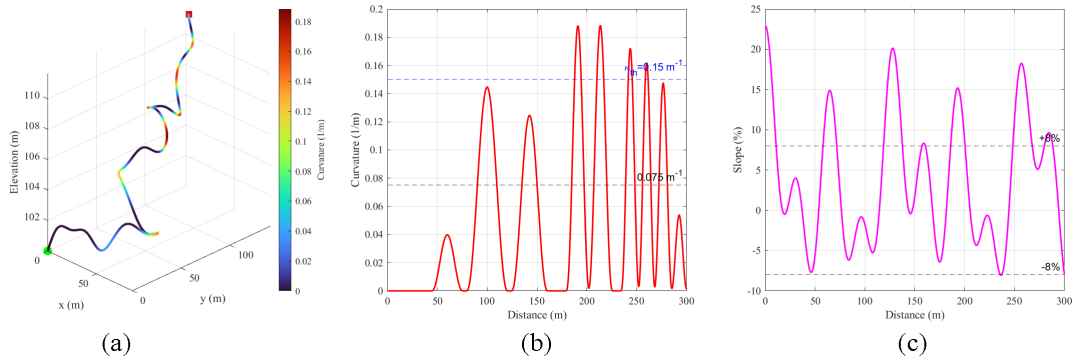


Figure 5. Synthetic benchmark trajectory and prescribed environmental conditions used for simulation evaluation: (a) three-dimensional trajectory, (b) path-curvature profile with supervisory thresholds, and (c) terrain-slope profile

All cases were evaluated under identical path, vehicle, controller, and simulation conditions. The primary metrics were RMS cross-track error, maximum cross-track error, accepted steering-mode transition count, and wheel-level steering-rate measures. Steering-transition smoothness was assessed using the RMS and maximum four-wheel steering rates within ± 0.5 s windows surrounding accepted transitions.

Disturbance recovery was evaluated under prescribed initial lateral offsets. A one-factor-at-a-time sensitivity analysis was conducted for turn-memory duration, recovery-memory duration, minimum dwell time, and velocity-scheduling gain scale while the remaining parameters were fixed at their nominal values. Recovery-memory sensitivity was evaluated under a 0.8 m initial lateral offset to activate the corresponding recovery behaviour. Trajectory responses, steering-mode histories, and commanded-velocity profiles were additionally used to support interpretation of the supervisory behaviour.

Particular emphasis was placed on the C7–C8 comparison to determine whether the temporal-memory states reduce unnecessary transitions, improve wheel-level steering continuity, and enhance trajectory-tracking consistency under otherwise identical conditions.

Statistical robustness was further evaluated using 20 paired Monte Carlo trials in which identical random initial lateral-position and heading perturbations were applied to C7 and C8. Initial lateral offsets were sampled from -0.8 to 0.8 m and initial heading offsets from $-8°$ to $8°$. Results were reported as mean $\pm$ standard deviation and evaluated using two-sided paired t-tests at $\alpha = 0.05$.

At each sampling instant, the supervisor evaluates a fixed number of filtered signals, threshold comparisons, memory counters, and priority rules. The per-step computational complexity is therefore $O(1)$, with no online optimisation, iterative numerical solution, or policy-network inference. Embedded execution time, processor utilisation, and memory consumption were not measured in the present simulation study.

3. RESULTS AND DISCUSSION

The proposed memory-aware supervisor was evaluated using the synthetic benchmark trajectory in Figure 5. The analysis considers trajectory tracking, steering transitions, wheel-level steering continuity, disturbance recovery, parameter sensitivity, and supporting velocity-scheduling behaviour.

3.1. Trajectory tracking and steering-transition performance

Figure 6 compares Fixed FWS (C1), Fixed CP4WS (C3), the non-memory supervisor (C7), and the proposed memory-aware supervisor (C8). All cases follow the reference path along straight segments, while clearer differences occur in regions containing rapid curvature changes. Fixed FWS exhibits larger local deviations because steering is restricted to the front axle, whereas Fixed CP4WS provides stronger turning response but cannot adapt its configuration to changing path conditions. In contrast, the supervisory strategies select steering modes according to the current trajectory and tracking demand.

The enlarged region in Figure 6 shows that C8 remains closer to the reference path than C7 during steering-mode activity.

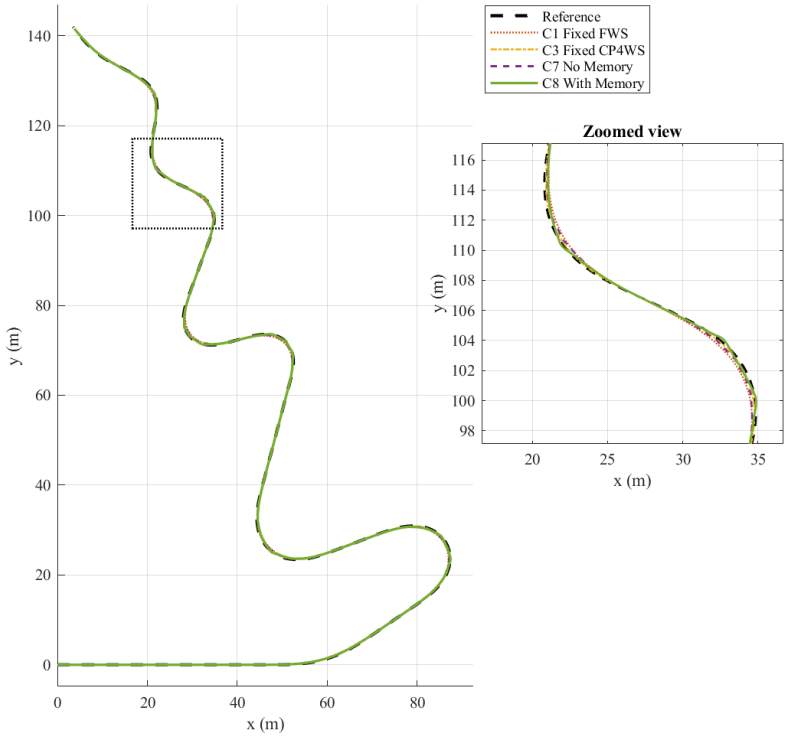


Figure 6. Full-path trajectory comparison for Fixed FWS (C1), Fixed CP4WS (C3), the non-memory supervisor (C7), and the memory-aware supervisor (C8)

The C7–C8 comparison in Figure 7 isolates the effect of temporal memory because both cases use identical path-tracking, steering-mapping, velocity-scheduling, vehicle, hysteresis, dwell-time, and simulation

settings. Figure 7(a) shows the cross-track error responses of C7 and C8. Figure 7(b) shows the accepted steering-mode transitions for both cases. The RMS CTE decreases from 0.2396 m to 0.1754 m, corresponding to a 26.8% reduction, while the maximum CTE decreases from 0.7296 m to 0.5670 m, corresponding to a 22.3% reduction. The number of accepted steering-mode transitions decreases from 126 to 71, representing a 43.7% reduction. The quantitative improvements in tracking accuracy and accepted steering-mode transitions are summarised in Table 6.

These results indicate that the memory-aware mechanism reduces premature mode release and repeated reactivation without sacrificing tracking performance.

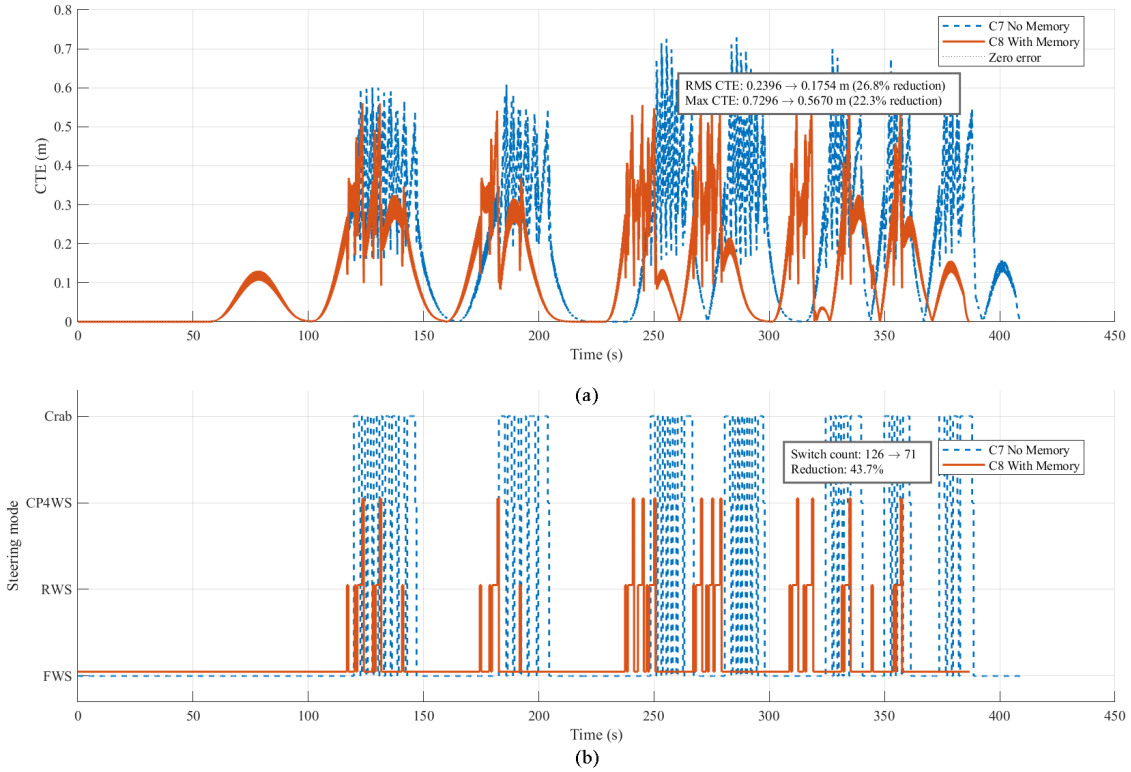


Figure 7. Comparison of the non-memory supervisor (C7) and memory-aware supervisor (C8): (a) cross-track-error response and (b) accepted steering-mode transitions

Table 6. Quantitative comparison of the non-memory and memory-aware supervisors

Metric	C7	C8	Change
RMS CTE (m)	0.2396	0.1754	-26.8%
Maximum CTE (m)	0.7296	0.5670	-22.3%
Accepted mode transitions	126	71	-43.7%

3.2. Wheel-level steering-transition behaviour

Wheel-level continuity was evaluated from the four individual steering angles. Steering rates were calculated from sample-to-sample wheel-angle changes, and transition-specific values were measured within ± 0.5 s windows surrounding accepted mode transitions.

Figure 8 compares the tracking and steering-transition performance of C7 and C8. Figure 8(a) shows RMS cross-track error, and Figure 8(b) shows the number of accepted steering-mode transitions. Figure 8(c) shows the RMS four-wheel steering rate within ± 0.5 s of accepted transitions, and Figure 8(d) shows the maximum four-wheel steering rate within the same windows. C8 reduced short-lived mode activations from 85 to 41, corresponding to a 51.8% reduction. The transition-window RMS wheel-steering rate decreased from 5.0103 rad/s to 3.8938 rad/s, while the maximum transition-window wheel-steering rate decreased from

127.8504 rad/s to 114.5911 rad/s. These changes correspond to reductions of 22.3% and 10.4%, respectively. Over the complete trajectory, the combined RMS wheel-steering rate decreased from 2.4176 rad/s to 1.4677 rad/s, representing a 39.3% reduction.

The results confirm that temporal memory reduces not only the frequency of accepted mode changes but also the aggregate wheel-steering activity associated with those changes.

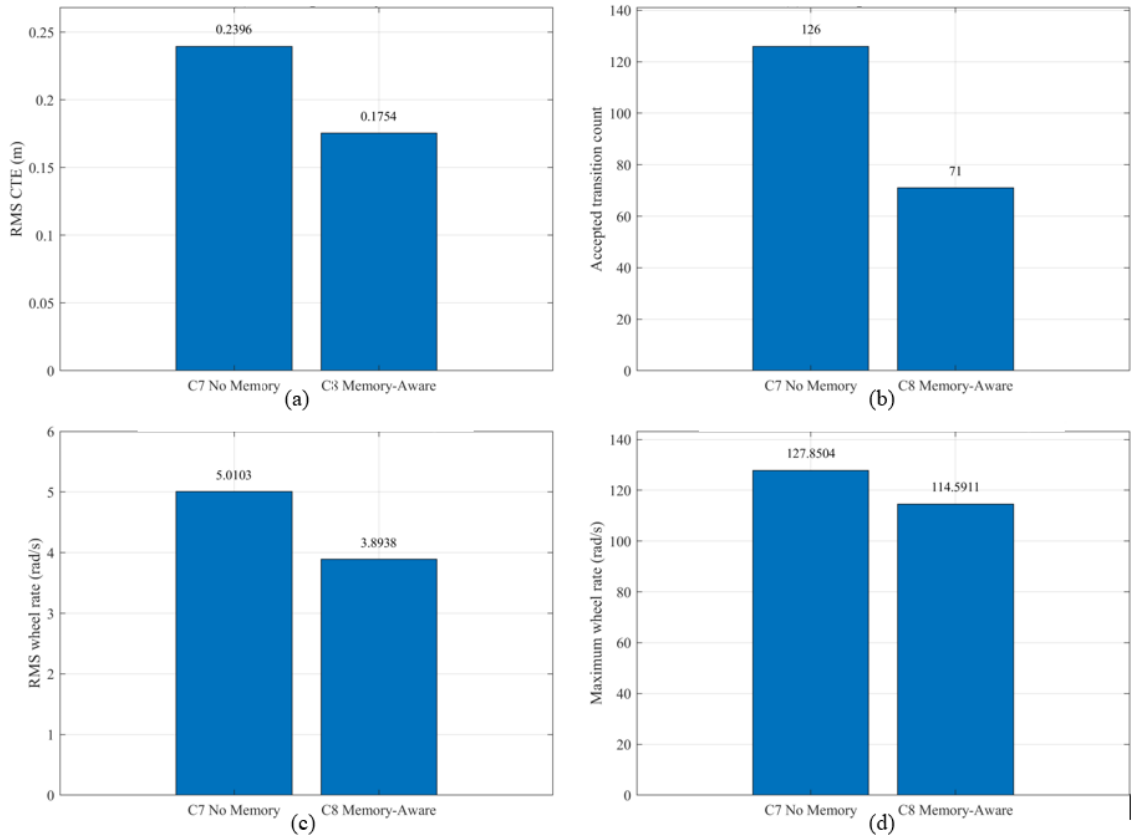


Figure 8. Comparison of C7 and C8: (a) RMS cross-track error, (b) accepted steering-mode transition count, (c) RMS four-wheel steering rate within ± 0.5 s of accepted transitions, and (d) maximum four-wheel steering rate within the same windows

3.3. Statistical validation under initial-condition perturbations

Statistical robustness was evaluated using 20 paired Monte Carlo trials. For each trial, identical random initial-condition perturbations were applied to C7 and C8 to preserve a matched comparison and isolate the effect of temporal memory. Initial lateral offsets were sampled from -0.8 m to 0.8 m, while initial heading offsets were sampled from $-8°$ to $8°$. Results are reported as mean $\pm$ standard deviation, and two-sided paired t-tests were performed at a significance level of $\alpha = 0.05$.

As summarised in Table 7, the mean RMS CTE decreased from 0.2392 ± 0.0017 m for C7 to 0.1783 ± 0.0032 m for C8, corresponding to a mean reduction of 25.5%. The mean maximum CTE decreased from 0.7385 ± 0.0372 m to 0.5948 ± 0.0771 m, representing a reduction of 19.7%. The mean accepted steering-mode transition count decreased from 123.4 ± 0.9 to 72.6 ± 1.7, corresponding to a reduction of 41.2%.

The transition-window RMS wheel-steering rate decreased from 5.0196 ± 0.0127 rad/s to 3.9128 ± 0.0334 rad/s, representing a 22.0% reduction. The corresponding maximum wheel-steering rate decreased from 127.8504 ± 0.0000 rad/s to 118.0441 ± 5.2871 rad/s, corresponding to a 7.7% reduction. All paired comparisons were statistically significant with $p < 0.001$, confirming that the tracking and steering-continuity improvements remained consistent under the tested initial-position and heading perturbations.

Table 7. Paired statistical comparison of C7 and C8 over 20 Monte Carlo trials

Metric	C7	C8	Reduction	p-value
RMS CTE (m)	0.2392 ± 0.0017	0.1783 ± 0.0032	25.5%	< 0.001
Maximum CTE (m)	0.7385 ± 0.0372	0.5948 ± 0.0771	19.7%	< 0.001
Accepted transitions	123.4 ± 0.9	72.6 ± 1.7	41.2%	< 0.001
Transition RMS rate (rad/s)	5.0196 ± 0.0127	3.9128 ± 0.0334	22.0%	< 0.001
Transition maximum rate (rad/s)	127.8504 ± 0.0000	118.0441 ± 5.2871	7.7%	< 0.001

3.4. Condition-dependent velocity-scheduling response

Figure 9 presents the supporting velocity-scheduling response. Figure 9(a) shows the commanded and mode-dependent velocities, and Figure 9(b) shows the individual speed-scheduler components. Figure 9(c) shows the selected steering mode, and Figure 9(d) shows the curvature severity and terrain slope. The commanded velocity remained between 0.614 and 0.799 m/s, with a mean of 0.774 m/s. The RMS sample-to-sample velocity change calculated using (10) was 0.00019 m/s.

The commanded velocity reflects the combined influence of the steering mode, curvature severity, cross-track error, heading error, and terrain slope. Speed reductions occur mainly during increased curvature severity and steering-mode activity. Because identical scheduling settings were applied to C7 and C8, the velocity response is treated as supporting system behaviour rather than an independent source of the observed memory-related improvements.

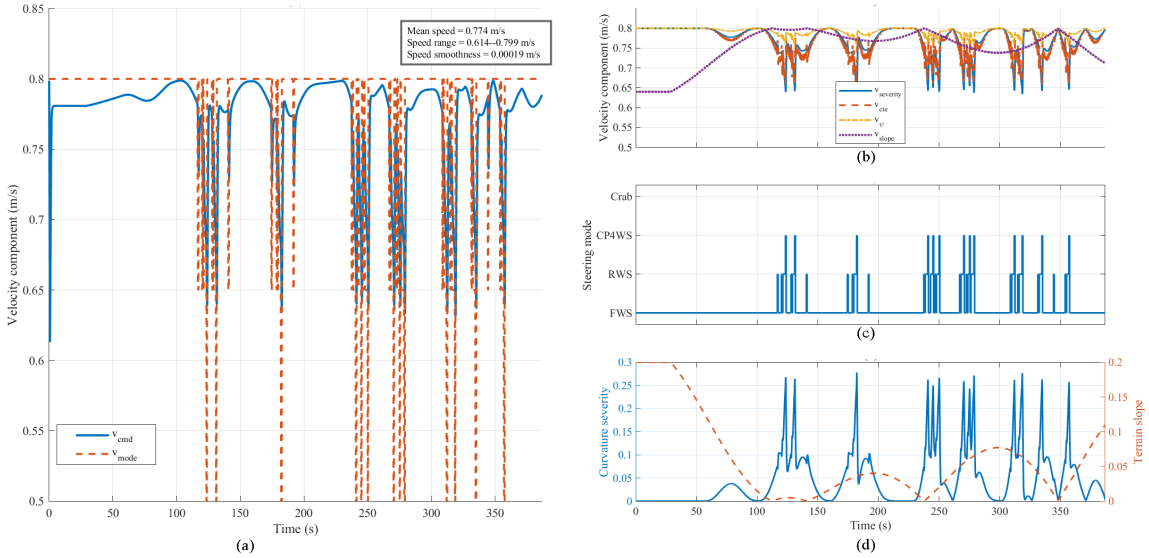


Figure 9. Condition-dependent velocity-scheduling response: (a) commanded and mode-dependent velocities, (b) individual speed-scheduler components, (c) steering-mode selection, and (d) curvature-severity and terrain-slope conditions

3.5. Robustness evaluation

Figure 10 compares recovery under initial lateral offsets of 0.2–0.8 m. Figure 10(a) shows the cross-track error response during recovery from a 0.8 m initial lateral offset. Figure 10(b) compares the RMS cross-track errors of C7 and C8 across initial lateral offsets from 0.2 to 0.8 m. Under the largest offset, C7 exhibits greater oscillatory correction because its steering decisions depend mainly on instantaneous conditions, whereas C8 retains recovery context through the recovery-memory state.

At a 0.8 m offset, RMS CTE decreases from 0.2441 m for C7 to 0.1850 m for C8, corresponding to a 24.2% reduction. Across all tested disturbances, C8 achieves improvements of 24.2% to 26.1%, indicating that memory-aware arbitration improves recovery robustness as disturbance severity increases.

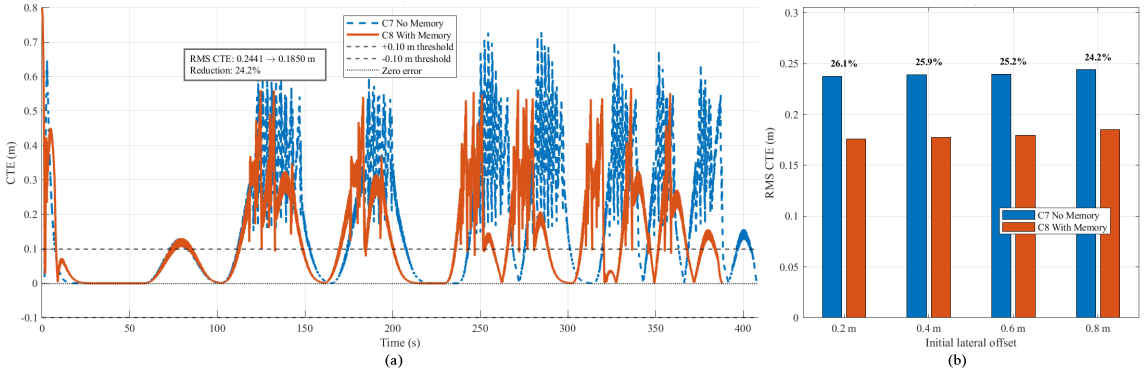


Figure 10. Recovery and robustness performance under initial lateral disturbances: (a) CTE recovery under a 0.8 m offset and (b) RMS CTE for offsets of 0.2 to 0.8 m

3.6. Parameter sensitivity analysis

A one-factor-at-a-time analysis was conducted for turn-memory duration, recovery-memory duration, minimum dwell time, and velocity-scheduling gain scale, with the remaining parameters fixed at their nominal values. Figure 11 summarises the results for all four parameters.

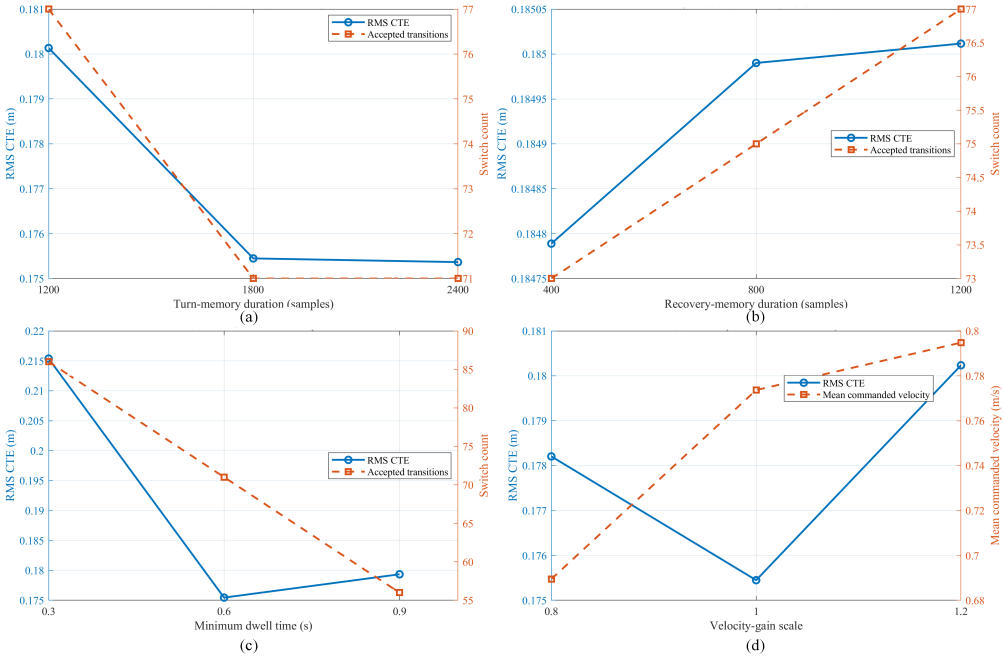


Figure 11. Sensitivity analysis of: (a) turn-memory duration, (b) recovery-memory duration under a 0.8 m initial lateral offset, (c) minimum dwell time, and (d) velocity-scheduling gain scale

The two memory parameters affected tracking error and transition count differently. In Figure 11(a), increasing the turn-memory duration from 1200 to 1800 samples reduced RMS CTE from 0.1801 m to 0.1754 m and accepted steering-mode transitions from 77 to 71. A further increase to 2400 samples yielded negligible improvement, so 1800 samples was selected. For recovery memory, Figure 11(b) shows the results under a 0.8 m initial lateral offset. RMS CTE stayed between 0.1848 and 0.1850 m, while the number of accepted transitions rose from 73 to 77 as the duration increased. The intermediate duration of 800 samples was retained to provide recovery support without excessive state retention.

Minimum dwell time also affected both tracking error and switching frequency. In Figure 11(c), increasing the dwell time from 0.30 to 0.60 s reduced RMS CTE from 0.2154 to 0.1754 m and accepted

transitions from 86 to 71. At 0.90 s, the transition count fell further to 56, while RMS CTE rose to 0.1793 m. The 0.60 s setting was therefore selected. For velocity scheduling, Figure 11(d) shows that a gain scale of 1.0 yielded the lowest RMS CTE of 0.1754 m, with a mean commanded velocity of 0.7737 m/s. Lower and higher gain scales did not improve the tracking–speed trade-off, so the nominal scale of 1.0 was retained.

3.7. Discussion of supervisory behaviour

The results show that temporal memory improves tracking consistency, reduces unnecessary steering transitions and wheel-level steering activity, and strengthens disturbance recovery. Curvature severity remains the primary supervisory variable, while turn memory and recovery memory preserve recent manoeuvring context after the triggering condition decreases. The velocity scheduler provides supporting speed reduction during increased manoeuvring demand.

3.8. Limitations and practical considerations

The study is limited to simulation using a low-speed kinematic model and a synthetic benchmark trajectory. Tyre-force dynamics, wheel slip, soil deformation, load transfer, steering-actuator delay, backlash, localisation uncertainty, delayed measurements, and higher-speed operation were not modelled. Although 20 paired Monte Carlo trials evaluated initial lateral-position and heading perturbations, sensor noise, terrain-estimation uncertainty, actuator variability, wheel-slip variation, and model-parameter uncertainty were not considered.

The selected thresholds, memory durations, dwell time, and velocity-scheduling settings are specific to the present vehicle geometry, sampling interval, operating-speed range, and benchmark trajectory. Other robotic platforms and operating environments may therefore require parameter retuning.

The quantitative comparison was limited to fixed steering modes and an equivalent adaptive supervisor without temporal memory. Comparisons with optimisation-based, fuzzy, and learning-based supervisors, field-derived trajectories, embedded execution-time assessment, and physical Pixkit validation remain future work.

4. CONCLUSION

This study proposed a memory-aware adaptive steering supervisor for low-speed agricultural mobile robots. Separate turn-memory and recovery-memory states were integrated with multi-mode steering arbitration, hysteresis, dwell-time protection, and condition-dependent velocity scheduling. Under the nominal benchmark, the proposed method reduced RMS cross-track error by 26.8%, maximum cross-track error by 22.3%, accepted steering-mode transitions by 43.7%, and transition-window RMS wheel-steering rate by 22.3% compared with the non-memory supervisor. Disturbance tests produced improvements of 24.2% to 26.1%. Across 20 paired Monte Carlo trials, RMS cross-track error, accepted transitions, and transition-window RMS steering rate were reduced by 25.5%, 41.2%, and 22.0%, respectively, with all paired comparisons significant at $p < 0.001$. These results show that retaining recent turning and recovery context improves tracking consistency, steering continuity, and disturbance recovery without online optimisation or learning-based policy inference. Future work will focus on broader uncertainty analysis, alternative supervisory comparisons, embedded implementation, field-derived trajectories, and physical-platform validation.

ACKNOWLEDGMENTS

The authors acknowledge the use of AI-assisted tools to improve the clarity and readability of this manuscript. All interpretations, findings, and conclusions remain the original work of the authors.

FUNDING INFORMATION

The authors express their gratitude to the Ministry of Higher Education (MOHE) for supporting this research under the LRGS grant LRGS/1/2025/UMPSA/02/2/1 (internal UMPSA ref: RDU250901).

AUTHOR CONTRIBUTIONS STATEMENT

This journal uses the Contributor Roles Taxonomy (CRediT) to recognize individual author contributions, reduce authorship disputes, and facilitate collaboration.

Name of Author	C	M	So	Va	Fo	I	R	D	O	E	Vi	Su	P	Fu
Athirah Najihah Zulkifili	✓	✓	✓	✓	✓	✓		✓	✓	✓	✓		✓	
Ismayuzri Ishak	✓	✓		✓			✓			✓		✓	✓	
Muhammad Aizzat Zakaria	✓	✓		✓			✓			✓		✓		
Chuan Yu	✓						✓			✓				
Beng Jin	✓						✓			✓				

C : **C**onceptualization
M : **M**ethodology
So : **So**ftware
Va : **Va**lidation
Fo : **Fo**rmal Analysis
I : **I**nvestigation
R : **R**esources
D : **D**ata Curation
O : Writing - **O**riginal Draft
E : Writing - Review & **E**diting
Vi : **Vi**sualization
Su : **Su**pervision
P : **P**roject Administration
Fu : **Fu**nding Acquisition

CONFLICT OF INTEREST STATEMENT

Authors state no conflict of interest.

DATA AVAILABILITY

The data that support the findings of this study are available from the corresponding author, Ismayuzri Ishak, upon reasonable request.

REFERENCES

[1] Y. Zhang, H. Liu, Y. Shen, S. He, H. Wang, and Y. Shen, "A systematic review of modeling and control approaches for path tracking in unmanned agricultural ground vehicles," *Agronomy*, vol. 15, no. 10, p. 2274, 2025, doi: 10.3390/agronomy15102274.

[2] C. Sun, J. Sun, S. Ding, Q. Li, and L. Ma, "Path tracking control in autonomous agricultural vehicles: A systematic survey of models, methods, and challenges," *Agriculture*, vol. 15, no. 23, p. 2522, 2025, doi: 10.3390/agriculture15232522.

[3] R. R. Shamshiri, *et al.* "Online path tracking with an integrated H∞ robust adaptive controller for a double-ackermann steering robot for orchard waypoint navigation," *International Journal of Intelligent Robotics and Applications*, vol. 9, no. 1, pp. 257–277, 2025, doi: 10.1007/s41315-024-00379-2.

[4] J. Dallas, M. P. Cole, P. Jayakumar, and T. Ersal, "Terrain adaptive trajectory planning and tracking on deformable terrains," *IEEE Transactions on Vehicular Technology*, vol. 70, no. 11, pp. 11255–11268, 2021, doi: 10.1109/TVT.2021.3114088.

[5] Z. Chen, J. Yin, S. M. Farhan, Z. Lin, and M. Zhou, "Adaptive path tracking control of unmanned agricultural machinery with fixed-time super-twisting sliding mode based on RLS-ELM," *Frontiers in Plant Science*, vol. 16, p. 1678648, 2025, doi: 10.3389/fpls.2025.1678648.

[6] K. Hu and W. Zhang, "Design and experiment of multi-mode steering system of agricultural machinery for hilly and mountainous area," *Advances in Mechanical Engineering*, vol. 13, no. 7, p. 16878140211034827, 2021, doi: 10.1177/16878140211034827.

[7] J. Qu, H. Li, Z. Zhang, X. Xi, R. Zhang, and K. Guo, "Performance analysis and optimization for steering motion mode switching of an agricultural four-wheel-steering mobile robot," *Agronomy*, vol. 12, no. 11, p. 2655, 2022, doi: 10.3390/agronomy12112655.

[8] N. T. Nguyen, P. Tej Gangavarapu, N. Mandel, R. Bruder, and F. Ernst, "Motion planning for 4WS Vehicle with autonomous Selection of steering modes via an MIQP-MPC controller," in *2024 IEEE International Conference on Robotics and Automation (ICRA)*, 2024, pp. 9765–9771, doi: 10.1109/ICRA57147.2024.10610461.

[9] B. Bae and D.-H. Lee, "Design of a four-wheel steering mobile robot platform and adaptive steering control for manual operation," *Electronics*, vol. 12, no. 16, p. 3511, 2023, doi: 10.3390/electronics12163511.

[10] N. Promkaew, N. Junhuathon, A. Phuphaphud, P. Kulvanit, and S. Sukpancharoen, "Enhanced pure pursuit with dynamic steering control for autonomous mobile robots and application to safe navigation in chemical plants," *Scientific Reports*, vol. 16, no. 1, p. 8820, 2026, doi: 10.1038/s41598-026-38695-1.

[11] M. Wang, C. Niu, Z. Wang, Y. Jiang, J. Jian, and X. Tang, "Model and parameter adaptive MPC path tracking control study of rear-wheel-steering agricultural machinery," *Agriculture*, vol. 14, no. 6, p. 823, 2024, doi: 10.3390/agriculture14060823.

[12] T. Baby, M. K. Gohil, and B. Bhattacharya, "Autonomous navigation of 4WIS4WID agricultural field mobile robot using deep reinforcement learning," *International Mechanical Engineering Congress and Exposition-India*, 2024.

[13] L. Hu, H. Cai, J. Huang, D. Cao, and X. Zhang, "The challenges of driving mode switching in automated vehicles: A review," *IEEE Transactions on Vehicular Technology*, vol. 73, no. 2, pp. 1777–1791, 2024, doi: 10.1109/TVT.2023.3319495.

[14] R. Bao, Y. Xu, L. Zhang, H. Yuan, J. Si, S. Wang, and T. Niu, "Deep reinforcement learning-based trajectory tracking framework for 4WS robots considering switch of steering modes," in *2025 IEEE/RSJ International Conference on Intelligent Robots and Systems (IROS)*, 2025, pp. 3792–3799, doi: 10.1109/IROS60139.2025.11247526.

[15] J. P. Hespanha, D. Liberzon, and A. Morse, "Hysteresis-based switching algorithms for supervisory control of uncertain systems," *Automatica*, vol. 39, no. 2, pp. 263–272, 2003, doi: 10.1016/S0005-1098(02)00241-8.

[16] X. Zhang, Y. Huang, S. Wang, L. Jiang, G. Li, and Y. Xie, "Hierarchical autonomous switching control of a multi-modes omnidirectional mobile robot," *Mechatronics*, vol. 80, p. 102692, 2021, doi: 10.1016/j.mechatronics.2021.102692.

[17] Y. Liu, J. Li, and D. Cong, "A seamless mode switching control method for independent metering controlled hydraulic actuator," *Technologies*, vol. 14, no. 1, p. 63, 2026, doi: 10.3390/technologies14010063.

[18] X. Chen, J. Cheng, H. Hu, G. Shao, Y. Gao, and Q. Zhu, "A novel fuzzy logic switched MPC for efficient path tracking of articulated steering vehicles," *Robotics*, vol. 13, no. 9, p. 134, 2024, doi: 10.3390/robotics13090134.
[19] D. Cui, C. K. Ahn, Y. Sun, and Z. Xiang, "Mode-dependent state observer-based prescribed performance control of switched systems," *IEEE Transactions on Circuits and Systems II: Express Briefs*, vol. 71, no. 8, pp. 3810–3814, 2024, doi: 10.1109/TCSII.2024.3370865.
[20] J. Nan, Z. Ge, X. Ye, A. F. Burke, and J. Zhao, "Model predictive control for autonomous vehicle path tracking through optimized kinematics," *Results in Engineering*, vol. 24, p. 103123, 2024, doi: 10.1016/j.rineng.2024.103123.
[21] R. Soitinaho and T. Oksanen, "Local navigation and obstacle avoidance for an agricultural tractor with nonlinear model predictive control," *IEEE Transactions on Control Systems Technology*, vol. 31, no. 5, pp. 2043–2054, 2023, doi: 10.1109/TCST.2023.3291533.
[22] J. d. A. Baltazar, A. L. d. F. Coelho, D. S. M. Valente, D. M. d. Queiroz, and F. M. d. M. Villar, "Development of a robotic platform with autonomous navigation system for agriculture," *AgriEngineering*, vol. 6, no. 3, pp. 3362–3374, 2024, doi: 10.3390/agriengineering6030192.
[23] M. Mammarella, L. Comba, A. Biglia, F. Dabbene, and P. Gay, "Cooperation of unmanned systems for agricultural applications: A theoretical framework," *Biosystems Engineering*, vol. 223, pp. 61–80, 2022, doi: 10.1016/j.biosystemseng.2021.11.008.
[24] Z. Yang, Y. Dai, M. Hu, Y. Bian, Q. Cui, and Y. Li, "Improving path tracking performance of 4wis vehicles via constraint-oriented consistent coordinated steering," *Chinese Journal of Mechanical Engineering*, vol. 38, no. 1, p. 158, 2025, doi: 10.1186/s10033-025-01298-4.
[25] Y. Wang, *et al.* "Coordination control for path tracking and stability of 4WS-4WID automated vehicles: A game theory-based approach," *IEEE Transactions on Vehicular Technology*, vol. 74, no. 5, pp. 7392–7403, 2025, doi: 10.1109/TVT.2025.3530102.
[26] L. Cui, F. Le, X. Xue, T. Sun, and Y. Jiao, "Design and experiment of an agricultural field management robot and its navigation control system," *Agronomy*, vol. 14, no. 4, p. 654, 2024, doi: 10.3390/agronomy14040654.
[27] S. Yim, "Comparison among active front, front independent, 4-wheel and 4-wheel independent steering systems for vehicle stability control," *Electronics*, vol. 9, no. 5, p. 798, 2020, doi: 10.3390/electronics9050798.
[28] D. Seo and J. Kang, "Controller design for active four-wheel steering and four-wheel independent drive-based mobile robot: Enhancing cornering performance in negative phase," *International Journal of Control, Automation and Systems*, vol. 23, no. 1, pp. 235–248, 2025, doi: 10.1007/s12555-024-0631-8.
[29] S. Kim, J. Lee, K. Han, and S. B. Choi, "Vehicle path tracking control using pure pursuit with MPC-based look-ahead distance optimization," *IEEE Transactions on Vehicular Technology*, vol. 73, no. 1, pp. 53–66, 2024, doi: 10.1109/TVT.2023.3304427.
[30] J. Wen, L. Yao, J. Zhou, Z. Yang, L. Xu, and L. Yao, "Path tracking control of agricultural automatic navigation vehicles based on an improved sparrow search-pure pursuit algorithm," *Agriculture*, vol. 15, no. 11, p. 1215, 2025, doi: 10.3390/agriculture15111215.
[31] C. Hu, *et al.* "Path tracking control for brake-steering tracked vehicles based on an improved pure pursuit algorithm," *Biosystems Engineering*, vol. 242, pp. 1–15, 2024, doi: 10.1016/j.biosystemseng.2024.04.006.
[32] Y. Xie, X. Zhang, S. Zheng, C. K. Ahn, and S. Wang, "Asynchronous H∞ continuous stabilization of mode-dependent switched mobile robot," *IEEE Transactions on Systems, Man, and Cybernetics: Systems*, vol. 52, no. 11, pp. 6906–6920, 2022, doi: 10.1109/TSMC.2021.3119054.
[33] C. Ju and H. I. Son, "A hybrid systems-based hierarchical control architecture for heterogeneous field robot teams," *IEEE Transactions on Cybernetics*, vol. 53, no. 3, pp. 1802–1815, 2023, doi: 10.1109/TCYB.2021.3133631.
[34] K. Xu, *et al.* "Performance-guaranteed adaptive switching fault-tolerant control of steer-by-wire system considering actuator fault and load disturbance," *IEEE Transactions on Transportation Electrification*, vol. 10, no. 4, pp. 8513–8527, 2024, doi: 10.1109/TTE.2024.3373890.
[35] S. Zhuang, H. Gao, and Y. Shi, "Model predictive control of switched linear systems with persistent dwell-time constraints: Recursive feasibility and stability," *IEEE Transactions on Automatic Control*, vol. 68, no. 12, pp. 7887–7894, 2023, doi: 10.1109/TAC.2023.3248279.
[36] Z. Peng, X. Song, S. Song, and V. Stojanovic, "Hysteresis quantified control for switched reaction–diffusion systems and its application," *Complex & Intelligent Systems*, vol. 9, no. 6, pp. 7451–7460, 2023, doi: 10.1007/s40747-023-01135-y.
[37] A. Nurkanovic and M. Diehl, "Continuous optimization for control of hybrid systems with hysteresis via time-freezing," *IEEE Control Systems Letters*, vol. 6, pp. 3182–3187, 2022, doi: 10.1109/LCSYS.2022.3181888.
[38] M. Marley, R. Skjetne, and A. R. Teel, "Hybrid control barrier functions for continuous-time systems," *IEEE Transactions on Automatic Control*, vol. 69, no. 10, pp. 6605–6619, 2024, doi: 10.1109/TAC.2024.3374265.
[39] C. Shen and J. Cheng, "Event-based sliding mode control for singularly perturbed systems with switching parameters," *ISA Transactions*, vol. 158, pp. 208–216, 2025, doi: 10.1016/j.isatra.2024.12.036.

BIOGRAPHIES OF AUTHORS



Athirah Najihah Zulkifili (Ph.D. Candidate) received the B.Comp.Sc. (Hons.) degree in software engineering from Universiti Malaysia Pahang Al-Sultan Abdullah in 2024, graduating with First-Class Honours. She is currently pursuing the Ph.D. degree at Universiti Malaysia Pahang Al-Sultan Abdullah, with a research focus on intelligent systems and autonomous mobile robots. Her research interests include vehicle kinematic modeling, adaptive control, robotics framework development, artificial intelligence, and computer vision. She aims to contribute to sustainable automation through the advancement of intelligent robotic systems. She can be contacted at email: zulkifiliathirah@gmail.com.



Ismayuzri Ishak received the B.Eng. (Hons.) and M.Eng. degrees in mechanical and manufacturing engineering from Universiti Malaysia Pahang Al-Sultan Abdullah in 2009 and 2013, respectively. He obtained his Ph.D. in 2018 from the Florida Institute of Technology, USA, focusing on a robotic FDM platform for multi-plane and 3D lattice structure printing. He is currently a Senior Lecturer with the Faculty of Manufacturing and Mechatronic Engineering Technology, Universiti Malaysia Pahang Al-Sultan Abdullah. His research interests include robotics, additive manufacturing, system integration, theoretical kinematics, and mechatronics. He has led and contributed to numerous research projects involving automation, IoT, and intelligent systems for industrial applications. He can be contacted at email: ismayuzri@umpsa.edu.my.



Muhammad Aizzat Zakaria received his B.Eng. and Ph.D. degrees from Universiti Teknologi Malaysia (UTM) in 2010 and 2015, specializing in autonomous vehicle engineering and trajectory tracking control. He is currently an Associate Professor with the Autonomous, Robotic and Control Lab, Faculty of Manufacturing and Mechatronic Engineering Technology, Universiti Malaysia Pahang Al-Sultan Abdullah (UMPSA), and is affiliated with the Centre for Advanced Industrial Technology. He also serves as the Director of the Centre for Innovation and Technology Transfer under the Research and Innovation Department, UMPSA. His research interests include autonomous and intelligent vehicles, vehicle stability and state monitoring, mechatronic systems, mobile robotics, ROS, and SLAM. He can be contacted at email: maizzat@umpsa.edu.my.



Chuan Yu is the Founder and Chief Executive Officer of PIX Moving and the President of Pixel Intelligence Co., Ltd., Tokyo, Japan. He received his Bachelor's degree in architecture design from Chongqing University, China, in 2000. He is an interdisciplinary innovator and technology entrepreneur specializing in autonomous mobility, digital fabrication, product innovation, and high-technology industrialization. Since founding PIX Moving in 2017, he has led the development of modular autonomous vehicle platforms for transportation, logistics, retail, and smart-city applications. His professional interests include autonomous mobility, modular vehicle platforms, digital manufacturing, innovative product development, and technology commercialization. Linkedin: https://www.linkedin.com/in/chuanyu. He can be contacted at email: angelo@pixmoving.com.



Beng Jin is the Lead Self-Driving Engineer at PIX Moving, with experience in developing autonomous driving systems using ROS and ROS 2. He leads the design and development of autonomous driving solutions for robotic mobility platforms, including logistics robots, retail robots, sweeping robots, and autonomous buses. His work focuses on autonomous vehicle software, robotic system integration, perception and control systems, and open-source driving platforms. He is also involved in developing the software, toolchain, and technical documentation for PixKit, which is based on the Autoware platform. His professional interests include autonomous driving, ROS/ROS2, Autoware, robotic mobility systems, and open-source vehicle technologies. Linkedin: https://www.linkedin.com/in/beng-jin-aa16a0242/?locale=en. He can be contacted at email: mark@pixmoving.net.